Mathematical Medicine and Biology (2017) **34**, 313–333
doi:10.1093/imammb/dqw010
Advance Access publication on June 8, 2016

Renal medullary and urinary oxygen tension during cardiopulmonary bypass in the rat

IOANNIS SGOURALIS*
National Institute for Mathematical and Biological Synthesis, NIMBioS, Knoxville, TN 37996, USA
*Corresponding author: Email: sgouralis@nimbios.org

ROGER G. EVANS
Cardiovascular Disease Program, Bioscience Discovery Institute and Department of Physiology, Monash University, Monash, Clayton, VIC 3800, Australia

AND

ANITA T. LAYTON
Department of Mathematics, Duke University, Duke, Durham, NC 27708, USA

[Received on 15 January 2016; revised on 12 April 2016; accepted on 11 May 2016]

Renal hypoxia could result from a mismatch in renal oxygen supply and demand, particularly in the renal medulla. Medullary hypoxic damage is believed to give rise to acute kidney injury, which is a prevalent complication of cardiac surgery performed on cardiopulmonary bypass (CPB). To determine the mechanisms that could lead to medullary hypoxia during CPB in the rat kidney, we developed a mathematical model which incorporates (i) autoregulation of renal blood flow and glomerular filtration rate, (ii) detailed oxygen transport and utilization in the renal medulla and (iii) oxygen transport along the ureter. Within the outer medulla, the lowest interstitial tissue P_{O2}, which is an indicator of renal hypoxia, is predicted near the thick ascending limbs. Interstitial tissue P_{O2} exhibits a general decrease along the inner medullary axis, but urine P_{O2} increases significantly along the ureter. Thus, bladder urinary P_{O2} is predicted to be substantially higher than medullary P_{O2}. The model is used to identify the phase of cardiac surgery performed on CPB that is associated with the highest risk for hypoxic kidney injury. Simulation results indicate that the outer medulla's vulnerability to hypoxic injury depends, in part, on the extent to which medullary blood flow is autoregulated. With imperfect medullary blood flow autoregulation, the model predicts that the rewarming phase of CPB, in which medullary blood flow is low but medullary oxygen consumption remains high, is the phase in which the kidney is most likely to suffer hypoxic injury.

Keywords: hypoxia; kidney; metabolism; cardiopulmonary bypass; cardiac surgery.

1. Introduction

Hospital-acquired acute kidney injury (AKI) is a serious clinical complication. In particular, patients who have undergone cardiac surgery that requires cardiopulmonary bypass (CPB) are at elevated risk of AKI (Karkouti *et al.*, 2009). Cardiac surgery on CPB may be associated with mismatched changes in renal oxygen delivery and oxygen consumption (Evans *et al.*, 2013). Mean arterial pressure is low during CPB (50–70 mmHg) (Andersson *et al.*, 1994), which is below the lower limit of renal autoregulation, i.e. during CPB kidneys are unable to maintain a stable blood flow. The resulting reduction in renal blood flow and thus oxygen supply (Andersson *et al.*, 1994) likely contributes to the risk of hypoxia and AKI.

Furthermore, the CPB circuit is primed with a blood cell free solution, resulting in haemodilution which limits the systemic and renal oxygen delivery even further (Rosner *et al.*, 2008).

Much of the oxygen consumed by the kidney is used to drive transport work, including the reabsorption of more than 99% of the filtered sodium under normal physiologic conditions. Renal blood flow is highly compartmentalized, with flow in the cortex (the outer portion of the kidney) substantially higher than that in the medulla (the innermost portion of the kidney). Blood flow is further compartmentalized within the medulla. The blood vessels that deliver oxygen to the medulla, i.e. the descending vasa recta (DVR), are sequestered within tightly packed vascular bundles, away from the renal tubules. This arrangement results in low oxygen tension (P_{O2}) outside the vascular bundles and contributes to the vulnerability of the medullary thick ascending limbs (TALs) of the loops of Henle to hypoxic injury. TALs have high metabolic demand due to the Na^+/K^+-ATPase pumps, which in fact account for the majority of the energy consumption in the renal medulla. Because the thick limbs are found outside of the vascular bundles, their oxygen supply is severely limited. When oxygen supply is reduced below normal, medullary hypoxic injury can develop. This is illustrated by the kidney's response to ischemia reperfusion which reveals widespread tubular epithelial necrosis and vascular congestion in the outer medulla (Brezis & Rosen, 1995; Okusa *et al.*, 1999). Thus, a goal of this study is to determine the medullary tissue oxygenation levels under physiological and surgical conditions.

Diagnosis of AKI is usually based on either an elevation of serum creatinine or the detection of oliguria (production of abnormally small amounts of urine) (Mehta & Chertow, 2003). Serum creatinine is a poor marker of early renal dysfunction, because serum concentration is greatly influenced by numerous non-renal factors (e.g. body weight, race, age, gender, total body volume, drugs, muscle metabolism and protein intake) (Bjornsson, 1979). The utility of serum creatinine is worse in the setting of surgery, because the patients are not in steady state; hence, serum creatinine lags far behind renal injury. As a result, substantial increases in serum creatinine are often not witnessed until 48–72 h after the initial insult to the kidney (Star, 1998; Mehta & Chertow, 2003). In addition, significant renal disease can exist with minimal or no change in creatinine clearance because of renal reserve, enhanced tubular secretion of creatinine or other factors (Bosch, 1995; Herrera & Rodríguez-Iturbe, 1998). Thus, serum creatinine is a poor biomarker of AKI and an alternative that is easily measured, unaffected by other biological variables and capable of both early detection and risk stratification would substantially assist the diagnosis of AKI.

It has been suggested that urine P_{O2} in the collecting ducts (CDs) would equilibrate with tissue P_{O2} of the inner medulla (Evans *et al.*, 2014). Accordingly, the P_{O2} of urine in the renal pelvis may change in response to stimuli that are expected to alter the oxygenation of the renal medulla. To investigate the potential of urinary P_{O2} as a biomarker of the risk of AKI in hospital settings, we use a mathematical model of the rat kidney and ureter to assess the extent to which urinary P_{O2} equilibrates with the inner medullary tissue P_{O2}. As previously noted, the renal structures that are most susceptible to hypoxic injuries are the TALs in the outer medulla (Fry *et al.*, 2014). Thus, a secondary goal of this study is to use model simulations to determine the relation between outer-medullary tissue P_{O2} and urinary P_{O2}.

In a recent study (Sgouralis *et al.*, 2015), we utilized a mathematical model of a single nephron to investigate the extent to which changes in systemic oxygenation during the surgical procedures performed on CPB might alter the medullary oxygenation. Simulations indicate that medullary oxygen extraction is substantially increased during the CPB rewarming phase. Because of the simplicity of that model we were unable to quantify oxygen levels in terms of medullary P_{O2}. By applying a much more detailed mathematical model of the renal medulla in this study, we aim to predict tissue and urine P_{O2} and to elaborate on our previous study.

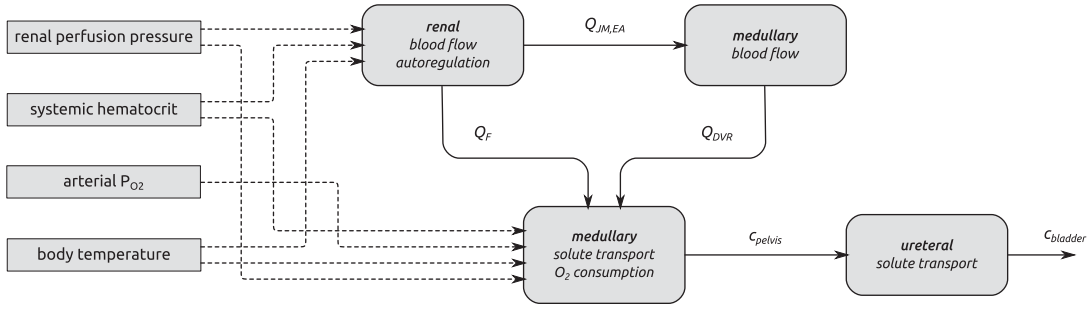

FIG. 1. A summary of the combined model. Q_F, glomerular filtration rate; $Q_{JM,EA}$, efferent arteriole blood flow of juxtamedullary nephrons; Q_{DVR}, DVR inflow; c_{pelvis}, pelvic, O_2 concentration; $c_{bladder}$, bladder O_2 concentration. For details see main text.

2. Mathematical model

The model represents solute transport in the renal cortex, medulla and ureter of the rat kidney and is based on our previously applied mathematical models of renal haemodynamics (Sgouralis & Layton, 2013, 2014), urine concentrating mechanism (Layton *et al.*, 2012; Moss & Layton, 2014), and oxygen transport (Fry *et al.*, 2014). We combined these models and extended the resulting model to represent oxygen transport along the ureter. For a schematic diagram illustrating the model components and key variables see Fig. 1. Below we highlight key model equations.

2.1 *Modelling renal blood flow and autoregulation*

The cortical component of the model simulates renal blood flow and autoregulation. The model represents afferent arterioles that respond to signals initiated by the *myogenic response* and *tubuloglomerular feedback*, which are triggered by variations in vascular blood pressure and macula densa Cl^- concentrations, respectively (Sgouralis & Layton, 2015a). The model afferent arterioles are formed by series of vascular smooth muscle cells, which set the local vascular tone. The local vascular tone may change when an activating signal, initiated by the autoregulatory mechanisms, perturbs the smooth muscle membrane potential. The vascular tone of the smooth muscles is the main determinant of the resistance of the afferent arteriole Ω_{AA}. Model details can be found in (Chen *et al.*, 2011; Sgouralis *et al.*, 2012; Sgouralis & Layton, 2014, 2015b).

Afferent arteriolar blood flow, Q_{AA}, is determined by pressure drop and vascular resistance according to Poiseuille's law

$$Q_{AA} = \frac{P_{RA} - P_D}{\Omega_{RA} + \Omega_{AA}} \tag{2.1}$$

where P_{RA} is the renal perfusion pressure (RPP), P_D is the blood pressure in the glomerular capillaries, Ω_{RA} is the resistance of the pre-afferent arteriole vasculature (assumed constant) and Ω_{AA} is the resistance of the afferent arteriole, Fig. 2. The latter depends on blood viscosity μ and the radius profile $R_{AA}(z)$ along the afferent arterioles

$$\Omega_{AA} = \int_{AA} \frac{8\mu\, dz}{\pi R_{AA}^4(z)}. \tag{2.2}$$

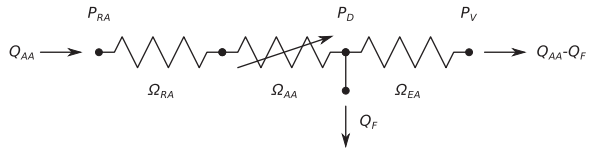

FIG. 2. Schematic diagram of the model vasculature. A pre-afferent arteriole vascular resistor (Ω_{RA}) delivers blood to the afferent arteriole (Ω_{AA}). At the glomerulus, which is located at the exit of the afferent arteriole, blood is divided between the proximal tubule of the associated nephron (not shown) and the efferent arteriole (Ω_{EA}). Q_{AA} and Q_F denote blood flow through the afferent arteriole and SNGFR, respectively. P_{RA}, P_D and P_V denote the renal perfusion pressure, glomerular capillary pressure and renal venous pressure, respectively.

Similarly, glomerular capillary pressure P_D is computed by Poiseuille's law, which, along the efferent arteriole, takes the form

$$P_D = P_V + (Q_{AA} - Q_F)\Omega_{EA}, \tag{2.3}$$

where P_V is the pressure in the renal vein (assumed constant), Q_F is the single nephron glomerular filtration rate (SNGFR) and Ω_{EA} is the resistance of the efferent arteriole.

2.2 *Modelling solute transport and oxygen consumption in the medulla*

Based on the predicted blood flow Q_{AA} and glomerular capillary pressure P_D, a glomerular filtration model (Sgouralis & Layton, 2014) is used to predict the SNGFR. The glomerular filtrate is fed into the proximal tubules of the nephrons. The model proximal tubules are assumed to reabsorb a fixed fraction of the filtered water and Na^+ load and to deliver the remaining load to the descending limbs of the model nephrons, which are located within the renal medulla (details can be found in Moss & Layton (2014)).

The medullary component of the model simulates tubular transport and oxygen consumption. The model includes loops of Henle, CDs and vasa recta. Tubules and vessels are represented as rigid tubes; some extending from the cortico-medullary boundary to the papillary tip (e.g. the CDs and the longest loops of Henle) and some extending from the cortico-medullary boundary and terminating within the medulla (e.g. the superficial or 'short' loops of Henle which turn at the outer-inner medullary boundary). The solutes explicitly considered in the model are Na^+, urea, deoxy- and oxy-haemoglobin (Hb and HbO_2), O_2, NO, HbNO and O_2^-. Together, the cortical and medullary components of the model predict steady-state fluid and solute flows along the renal tubules and interstitial tissue P_{O2} at all levels of the medulla.

Detailed transport equations can be found in our previous study (Fry *et al.*, 2015) and the references therein. In general, conservation of solute k along a tubule or vessel i is given by

$$A_i \frac{\partial c_{i,k}}{\partial t} = -\frac{\partial}{\partial x}\left(Q_i c_{i,k}\right) - J_{i,k} - R_{i,k}, \tag{2.4}$$

where $c_{i,k}$ denotes solute concentration, Q_i denotes fluid flow, A_i denotes tubular cross-sectional area and $J_{i,k}$ denotes transmural solute flux. For a non-reactive solute (e.g. Na^+ and urea), the reaction term $R_{i,k}$ is set to zero; for others, $R_{i,k}$ includes production, consumption and biochemical reactions.

Along some of the nephron segments, e.g. the proximal straight tubules (PSTs), TALs and CDs, Na^+ is actively reabsorbed via basolateral Na^+/K^+-ATPase pumps. The model assumes that T_{Na}-to-Q_{O_2} (TQ,

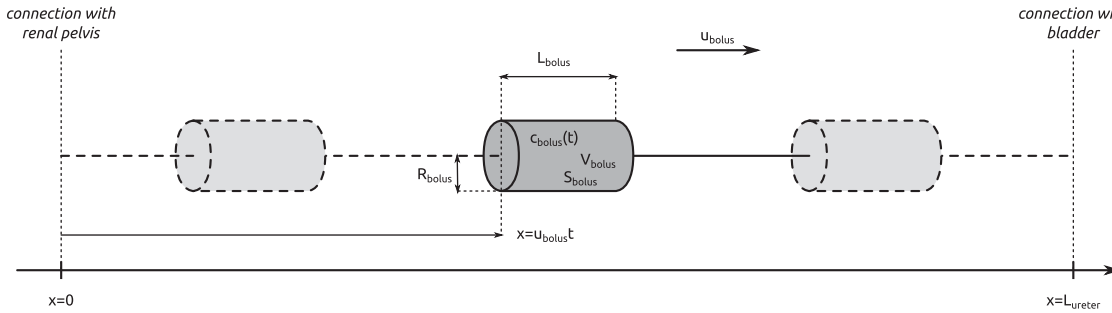

FIG. 3. Schematic diagram of the model ureter. Peristaltic boluses of volume V_{bolus} and contact area S_{bolus} travel from the renal pelvis (left) to the bladder (right) at a speed u_{bolus}. L_{bolus} and R_{bolus} characterize the bolus' dimensions.

where T_{Na} denotes the moles of Na^+ transported and Q_{O_2} denotes the moles of oxygen consumed) ratios are fixed at 18 for the TALs and PSTs and 12 for the CDs, based on tubular epithelial transport simulations (Weinstein, 1998; Nieves-Gonzalez *et al.*, 2013). We further assume that below some critical P_{O2} (denoted $P_{i,c}$ for tubule i), anaerobic metabolism maintains some fraction (denoted F_{AN}) of the energy required to actively transport Na^+. The rate of active oxygen consumption in the epithelia of the PSTs, TALs and CDs is then given by

$$R_{i,\text{O}_2}^{\text{active}} = \frac{2\pi r_i}{A_i^{\text{epi}}} \frac{\Psi_{i,\text{Na}}^{\text{active}}}{TQ_i} \Theta(P_{i,\text{O}_2}), \tag{2.5}$$

where TQ_i is the TQ ratio, $\Psi_{i,\text{Na}}^{\text{active}}$ is the Na^+ active transport rate and $\Theta(P_{i,\text{O}_2})$ is the fraction that is supported by aerobic respiration. The latter is given by

$$\Theta(P_{i,\text{O}_2}) = \begin{cases} 1, & P_{i,\text{O}_2} \geq P_{i,c} \\ \frac{P_{i,\text{O}_2}/P_{i,c}}{F_{\text{AN}}+(1-F_{\text{AN}})(P_{i,\text{O}_2}/P_{i,c})}, & P_{i,\text{O}_2} < P_{i,c}. \end{cases} \tag{2.6}$$

The active Na^+ transport rate $\Psi_{i,\text{Na}}^{\text{active}}$ is characterized by Michaelis–Menten kinetics

$$\Psi_{i,\text{Na}}^{\text{active}} = V_{\max,i,\text{Na}} \frac{c_{i,\text{Na}}(x)}{K_{\text{M,Na}} + c_{i,\text{Na}}(x)}, \tag{2.7}$$

where $V_{\max,i,\text{Na}}$ is the maximal rate of Na^+ transport (in unit of nmol/(cm^2 s)) and $K_{\text{M,Na}}$ is the Michaelis constant (in unit of mM).

2.3 *Modelling solute transport along the ureter*

To predict bladder urinary P_{O2}, we extended the renal model to represent oxygen transport along the ureter. The model ureter extends between $x = 0$ (connection with the renal pelvis) and $x = L_{\text{ureter}}$ (connection with the bladder); see Fig. 3. Urine is transported along the ureter in boluses by peristaltic pumping of the ureter walls. The ureter is water impermeable (Kreft *et al.*, 2010); thus, as the urine bolus moves through the ureter, its volume (V_{bolus}) remains unchanged. In contrast, oxygen may diffuse across the ureter epithelium. We assume a uniform oxygen concentration in the urine bolus, denoted c_{bolus} and

seek to track its change as the bolus moves from the CD (i.e. renal pelvis) to the bladder. Bolus oxygen conservation is given by

$$V_{\text{bolus}} \frac{dc_{\text{bolus}}(t)}{dt} = \kappa_{\text{O2}} S_{\text{bolus}} (c_{\text{ureter}} - c_{\text{bolus}}(t)), \tag{2.8}$$

where c_{ureter} is the oxygen concentration along the ureter walls, assumed uniform throughout the length of the ureter. S_{bolus} denotes the surface area of the bolus, and κ_{O2} is the oxygen permeability of the ureter epithelium. The initial time ($t = 0$) is taken to be the time that the bolus exits the collecting duct. Thus $c_{\text{bolus}}(0)$ is equal to the oxygen concentration of the CD outflow (denoted c_{pelvis}), which is predicted by the medullary model.

We assume that the bolus travels at a uniform speed of u_{bolus}, which corresponds to the speed of the peristaltic wave. Thus, the time needed for a bolus to reach the bladder is $t_{\text{transit}} = L_{\text{ureter}}/u_{\text{bolus}}$. Integrating (2.8), we determine the urinary oxygen concentration in the bladder (i.e. $c_{\text{bolus}}(t_{\text{transit}})$, denoted c_{bladder}) to be

$$c_{\text{bladder}} = c_{\text{ureter}} + (c_{\text{pelvis}} - c_{\text{ureter}}) \exp\left(-\kappa_{\text{O2}} \frac{S_{\text{bolus}}}{V_{\text{bolus}}} \frac{L_{\text{ureter}}}{u_{\text{bolus}}}\right). \tag{2.9}$$

If one assumes that the model bolus is a column of fluid with radius R_{bolus} and length L_{bolus}, as shown on Fig. 3, then $S_{\text{bolus}} = 2\pi R_{\text{bolus}} L_{\text{bolus}}$ and $V_{\text{bolus}} = \pi (R_{\text{bolus}})^2 L_{\text{bolus}}$, which implies $S_{\text{bolus}}/V_{\text{bolus}} = 2/R_{\text{bolus}}$. Thus, (2.9) becomes

$$c_{\text{bladder}} = c_{\text{ureter}} + (c_{\text{pelvis}} - c_{\text{ureter}}) \exp\left(-\frac{2\kappa_{\text{O2}}}{R_{\text{bolus}}} \frac{L_{\text{ureter}}}{u_{\text{bolus}}}\right). \tag{2.10}$$

Typical values for the rat ureter are $L_{\text{ureter}} = 3.4$ cm (Onyeanusi *et al.*, 2009) and $u_{\text{bolus}} = 8.12$ mm/s (Tillig & Constantinou, 1996). We use $c_{\text{ureter}} = 0.04$ mM that corresponds to a tissue P_{O2} of 30 mmHg. Oxygen permeability is computed by $\kappa_{\text{O2}} = D_{\text{O2}}/h_{\text{epith}}$, where $D_{\text{O2}} = 2.4 \times 10^{-5}$ cm^2/s is the oxygen diffusion coefficient, and $h_{\text{epith}} = 0.06$ mm is the thickness of the ureter epithelium in rats (Wolf *et al.*, 1996). Bolus radius R_{bolus} is taken to be 0.36 mm, which, given a baseline urine flow of 2.56×10^{-2} ml/min, as predicted by the medullary model at baseline, corresponds to a bolus length of 3.1 mm (Tillig & Constantinou, 1996).

2.4 *Modelling medullary blood flow*

A major determinant of medullary oxygen levels is medullary blood flow, which is modulated by vasopressin, the antidiuretic hormone (Cowley, 2000). The degree to which medullary blood flow is autoregulated appears to depend on the hydration status of the animal (Cupples & Marsh, 1988; Roman *et al.*, 1988; Mattson *et al.*, 1991, 1993; Franchini *et al.*, 1997), and has not been well characterized for patients or animals undergoing surgery performed under CPB. Given that uncertainty, we assume that medullary blood flow depends linearly on the efferent arteriole blood flow of the juxtamedullary nephrons, denoted $Q_{\text{JM,EA}}$, which the oxygen-supplying DVR stem from. That is, DVR inflow (specified at the cortico-medullary boundary) is given by

$$Q_{\text{DVR}} = Q^{\text{ref}}_{\text{DVR}} \left(1 + \frac{\beta}{Q^{\text{ref}}_{\text{JM,EA}}} \left(Q_{\text{JM,EA}} - Q^{\text{ref}}_{\text{JM,EA}}\right)\right). \tag{2.11}$$

The reference DVR flow $Q^{\text{ref}}_{\text{DVR}}$ and juxtamedullary efferent arteriolar flow $Q^{\text{ref}}_{\text{JM,EA}}$ are taken to be 8 and 300 nl/min, respectively, in agreement with the baseline values of our previous modelling study (Fry *et al.*, 2014). The case where $\beta = 0$ corresponds to perfect autoregulation of medullary blood flow, in which Q_{DVR} is independent of renal blood flow. The case where $\beta = 100\%$ corresponds to complete absence of medullary blood flow autoregulation, in which Q_{DVR} depends on renal blood flow.

2.5 *Modelling the effects of hypothermia*

During the main phase of the cardiac surgery, the patient's body temperature is usually lowered (Andersson *et al.*, 1994). Body temperature has multiple systemic and renal effects, as discussed in Sgouralis *et al.* (2015). Notably, body temperature has a profound effect on the metabolic rate. In the context of renal function, body temperature affects the active reabsorption of Na^+. This is represented in the model as a linear dependence of the maximum transport rate, i.e. $V_{\text{max},i,\text{Na}}$ in (2.7), on body temperature (T):

$$V_{\text{max},i,\text{Na}} = V^{\text{ref}}_{\text{max},i,\text{Na}}(1 + s_{\text{T}}(T - T^{\text{ref}})), \tag{2.12}$$

where $V^{\text{ref}}_{\text{max},i,\text{Na}}$ denotes the maximum Na^+ transport rate at a baseline body temperature of $T^{\text{ref}} = 37°\text{C}$ and s_{T} characterizes the sensitivity to T. We use $s_{\text{T}} = 0.056/°\text{C}$ such that the predicted Na^+ excretion at 28°C increases ∼3.1-fold from baseline, consistent with the experimental data in Broman & Källskog (1995).

Other temperature-dependent effects of hypothermia that are incorporated in the model include (i) elevation of afferent arteriole myocyte cytosolic $[Ca^{2+}]$, which affects the vascular tone of the afferent arteriolar smooth muscles and thus the resistance Ω_{AA}; (ii) vasoconstriction of the efferent arteriole, which affects efferent arteriole vascular resistance Ω_{EA}; (iii) increase in plasma and tubular fluid viscosities, which also affects afferent and efferent arteriole vascular resistances Ω_{AA} and Ω_{EA} as well as glomerular filtration and (iv) decrease in glomerular ultrafiltration coefficient, which also affects glomerular filtration (Broman & Källskog, 1995). A detailed description of how these effects are modelled can be found in Sgouralis *et al.* (2015).

We have validated our approach of modelling hypothermia; a detailed summary of model predictions and a comparison with the available data reported in Broman & Källskog (1995) can be found in the Supplemental Materials.

3. Results

3.1 *Baseline predictions*

We first compute model solutions for a rat kidney, in anti-diuretic status, under baseline haemodynamics conditions (for haemodynamics parameters see Table 1, column labelled 'Baseline'). Figure 4a shows medullary P_{O2} profiles for the interstitial fluid near the long DVR (which are located centrally within the vascular bundles; curve labelled 'VB'), for the interstitial fluid exterior to the vascular bundles (where the medullary TALs are located; curve labelled 'ext-VB') and for the luminal fluid along the CD (curve labelled 'CD').

We first consider the *outer medulla* (i.e. upper 2 mm of the medulla). Because of the sequestration of the DVR within the vascular bundles, away from the TALs which have high metabolic demands, a substantial P_{O2} radial gradient can be observed in the outer medulla, as indicated by the difference

TABLE 1 *Summary of simulated baseline and CPB phases. These values are typical of those encountered during CPB surgery (Andersson et al., 1994).*

Parameter	Baseline	Pre-CPB	Hypo-CPB	Rewarm-CPB	Post-CPB	Units
RPP	100	75	50	50	75	mmHg
Arterial P_{O2}	100	100	400	400	100	mmHg
Systemic hematocrit	45	45	25	25	25	%
Body temperature	37	37	28	37	37	°C

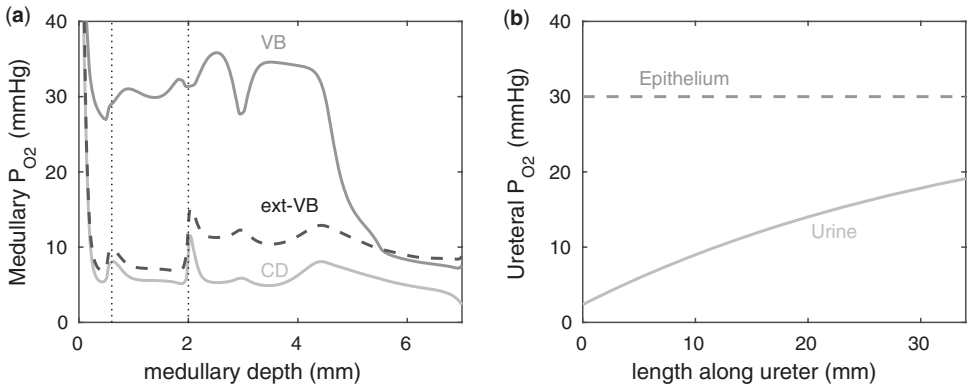

FIG. 4. Baseline model predictions. (a) Interstitial fluid P_{O2} profiles in selected regions along the model medulla: VB, interstitial fluid P_{O2} within the vascular bundles; Ext-VB, interstitial fluid P_{O2} external to the vascular bundles and CD, collecting duct luminal fluid P_{O2}. Dotted lines indicate the boundaries of inner/outer stripes (at $x = 0.6$ mm) and inner/outer medulla (at $x = 2$ mm). (b) Urine P_{O2} along the ureter. Dashed line indicates P_{O2} along the ureter walls.

between interstitial fluid P_{O2} inside and outside the vascular bundle (compare 'VB' and 'ext-VB'). In the outer medulla, the lowest interstitial P_{O2}, which is 6.8 mmHg, is predicted in the interbundle region in inner stripe (i.e. upper 0.6 mm).

In the *inner medulla* (i.e. the lower 5 mm of the medulla), the thin ascending limbs do not engage in active Na^+ transport. Nonetheless, a P_{O2} radial gradient can also be found in the upper inner medulla, where the DVR are separated from the CDs that have substantial Na^+/K^+-ATPase activities. In the lowest 1.5 mm of the inner medulla, the arrangement of tubules and vessel becomes homogeneous (Pannabecker *et al.*, 2004) and the P_{O2} radial gradient vanishes. The CD luminal fluid P_{O2} varies substantially along the inner medulla, decreasing from 5.2 mmHg near the inner-outer medullary boundary to 2.4 mmHg at the papillary tip (i.e. the lowest point in medulla).

Figure 4b shows urinary P_{O2} along the *ureter*. The ureter is contiguous with the inner-medullary CD, thus urinary P_{O2} at the ureter entrance is the same as that of CD outflow. Because the ureter is situated in a well-perfused region, the P_{O2} of the ureter walls is relatively high, at 30 mmHg. The resulting diffusive entry of oxygen raises urinary P_{O2} from 2.4 to 19.1 mmHg within the bladder. Thus, baseline bladder P_{O2} is 12.3 mmHg higher than the lowest interstitial P_{O2} in the inner stripe. That difference is attributed in large part to the P_{O2} increase in the urine as it travels along the ureter.

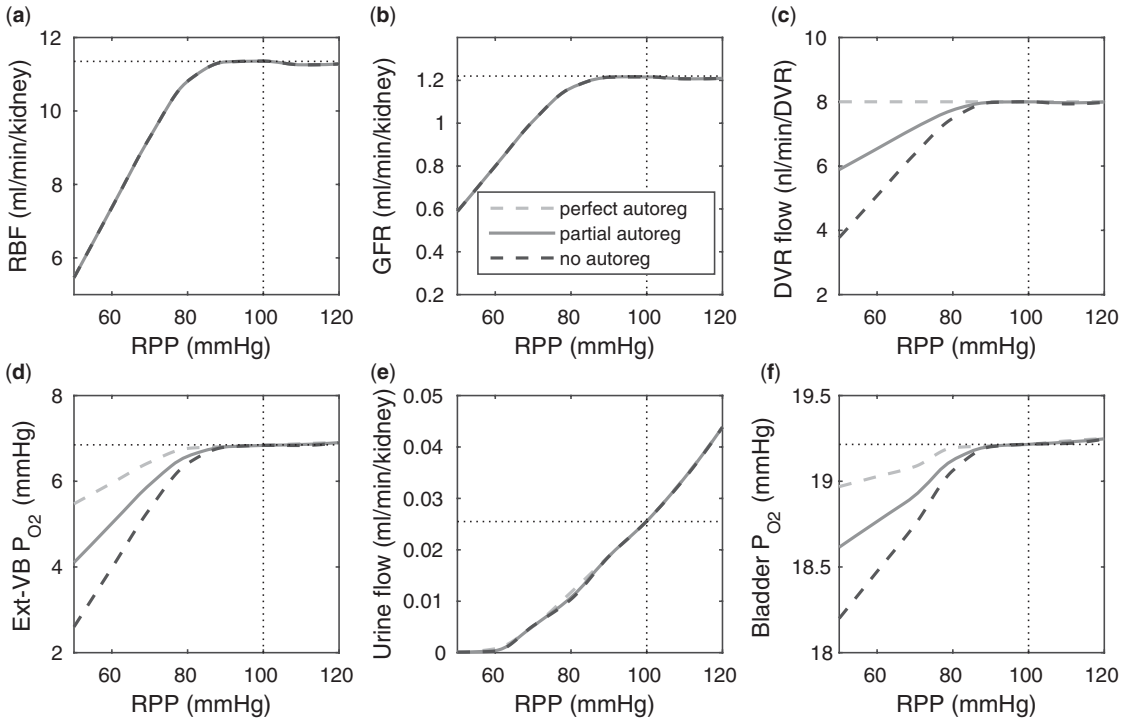

FIG. 5. Effects of variations in RPP on: (a), renal blood flow; (b) glomerular filtration rate; (c) DVR flow at the cortico-medullary boundary; (d) interstitial fluid P_{O2} in the lower inner stripe outside the vascular bundles; (e) urine flow and (f) urinary P_{O2} in the bladder. Results were computed for three different scenarios of medullary blood flow autoregulation. Dotted lines indicate baseline values.

3.2 *Effects of systemic factors on renal function and oxygenation*

In the next set of simulations, we investigate the effects of varying systemic factors on renal blood flow, renal oxygenation and urinary P_{O2}. Specifically, we consider the effects of RRP (P_{RA} in (2.1)), systemic haematocrit (the fraction of arterial blood Q_{AA} that is accounted for by red blood cells), arterial P_{O2} and body temperature; these parameters correspond to haemodynamics factors that play a key role in renal health following cardiac surgery under CPB (Andersson *et al.*, 1994; Sgouralis *et al.*, 2015). Given the uncertainty in the degree of medullary blood flow autoregulation (see Section 2.4), we consider three cases: *Case 1*, where we assume perfect autoregulation of medullary blood flow by setting $\beta = 0$ in (2.11) (referred to as 'perfect autoreg'); *Case 2*, where we set $\beta = 50\%$, leading to imperfect medullary blood flow autoregulation ('partial autoreg') and *Case 3*, where we assume no autoregulation so that medullary blood flow changes proportionally to renal blood flow by setting $\beta = 100\%$ ('no autoreg').

Renal perfusion pressure. We varied RPP over the range of 50–120 mmHg. For RPP above ~80 mmHg, the autoregulatory response of the afferent arterioles sufficiently compensates to maintain a stable renal blood flow and glomerular filtration rate (see Fig. 5a and b), resulting in essentially no change in medullary oxygenation and urinary P_{O2} (Fig. 5d and f). The increase in urine flow as RPP increases (Fig. 5e) is due

to the pressure natriuresis/diuresis response, which reduces proximal tubule Na^+ and water reabsorption as blood pressure increases. For RPP above 80 mmHg, all three cases predict essentially the same trends.

For RPP below 80 mmHg, the afferent arterioles' autoregulatory response fails to completely compensate, resulting in lower arteriolar flow, glomerular filtration rate and urine flow (Fig. 5a, b, and e). The effect on medullary oxygenation depends on how medullary blood flow is regulated (compare the three curves in Fig. 5c). As RPP is reduced, medullary and urine P_{O2} decrease less drastically when medullary blood flow is better regulated (Fig. 5d and f). In particular, although in the 'no autoreg' case bladder urinary P_{O2} decreases approximately linearly from 19.3 to 18.3 mmHg as RPP decreases from 100 to 50 mmHg, the 'perfect autoreg' case and, to a lesser extent, the 'partial autoreg' case predict lower changes in bladder's urinary P_{O2} ($\sim$0.3 and $\sim$0.5 mmHg, respectively, see Fig. 5f).

Systemic hematocrit. As in our previous study (Sgouralis *et al.*, 2015), we assume a linear relationship between systemic and medullary hematocrits, denoted $\mathrm{Htc}_{\mathrm{SYS}}$ and $\mathrm{Htc}_{\mathrm{MED}}$, respectively. Given that under baseline conditions, $\mathrm{Htc}_{\mathrm{MED}} = 0.25$ and $\mathrm{Htc}_{\mathrm{SYS}} = 0.45$, we assume that systemic and medullary hematocrits vary *in tandem* according to

$$\frac{\mathrm{Htc}_{\mathrm{MED}}}{\mathrm{Htc}_{\mathrm{SYS}}} = \frac{0.25}{0.45}. \tag{3.1}$$

Key model results are shown in Fig. 6. A higher hematocrit leads to elevated blood viscosity (Pries *et al.*, 1994) and thus reduced blood flow (Fig. 6a), lower glomerular filtration (Fig. 6b), and lower urine flow (Fig. 6e). It is noteworthy that the 'perfect autoreg' and the 'no autoreg' cases predict different trends in medullary and urinary P_{O2}. Increasing hematocrit in the 'no autoreg' case has two competing effects on medullary oxygenation: the elevated blood viscosity reduces arteriolar flow and thus medullary blood flow (Fig. 6c), but the oxygen-carrying capacity of the blood is increased. These two opposing effects result in limited changes in medullary and bladder P_{O2}; see Fig. 6d and f. In contrast, when medullary blood flow is fixed (in the 'perfect autoreg' case), a higher hematocrit increases medullary oxygen delivery, resulting in elevated medullary and urinary P_{O2}; see Fig. 6c and f. Predictions of the 'partial autoreg' case lie between the two extreme cases.

Arterial P_{O2}. To model the effects of arterial P_{O2}, we assume that plasma and RBC P_{O2} of the model DVR depend linearly on the P_{O2} of the arterial blood. We assume that under baseline conditions, DVR plasma and RBC P_{O2} (denoted P_{O2}^{DVR}) is 60% that of the arterial blood P_{O2} (denoted P_{O2}^{SYS}) (Chen *et al.*, 2009). When arterial P_{O2} deviates from its baseline value, DVR P_{O2} varies proportionally, i.e. $P_{O2}^{\mathrm{DVR}} = 0.6P_{O2}^{\mathrm{SYS}}$. Arterial P_{O2} was varied from 75 to 400 mmHg; key model results are shown in Fig. 7.

Because arterial P_{O2} has no effect on renal blood flow (Fig. 7a), all three cases predict essentially the same results: glomerular filtration rate, medullary blood flow, and urine flow are minimally affected by variations in arterial P_{O2} (Fig. 7b, c, and e), whereas medullary P_{O2} and urinary P_{O2} increase as arterial P_{O2} increases (Fig. 7d and f).

Body temperature. Key simulation results that characterize the effects of body temperature on medullary oxygenation and renal function are shown in Fig. 8. At cooler temperatures, blood viscosity increases and vascular smooth muscles constrict (Broman & Källskog, 1995; Sgouralis *et al.*, 2015), resulting in reduced blood flow (see Fig. 8a) and GFR (see Fig. 8b). But, perhaps more importantly, the body's metabolism slows down at lower temperatures. In the context of renal function, this leads to reduced

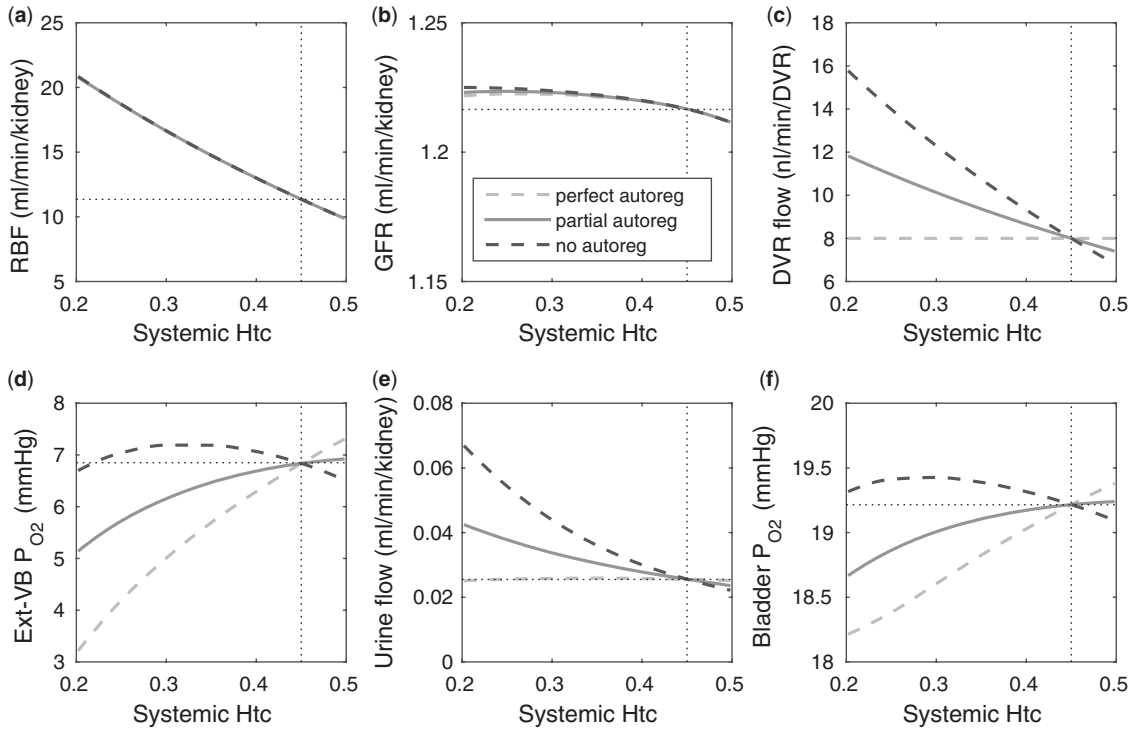

FIG. 6. Effects of variations in systemic hematocrit (Htc) on: (a) renal blood flow; (b) glomerular filtration rate; (c) DVR flow at the cortico-medullary boundary; (d) interstitial fluid P_{O2} in the lower inner stripe outside the vascular bundles; (e) urine flow and (f) urinary P_{O2} in the bladder. Results were computed for three different scenarios of medullary blood flow autoregulation. Dotted lines indicate baseline values.

active Na^+ transport rate, which impedes water withdrawal from the CD, resulting in higher urine flow (Fig. 8e).

Interestingly, the 'perfect autoreg' case and the 'no autoreg' case predict opposite effects on medullary and urinary P_{O2} as body temperature is lowered. As previously noted, the active Na^+ transport rate and the associated oxygen consumption decrease at lower temperature. Thus, in the 'perfect autoreg' case, where medullary blood flow and oxygen supply are fixed, medullary P_{O2} doubles and urinary P_{O2} increases by $\sim$1 mmHg as temperature decreases from 37 to 28°C. In contrast, in the 'no autoreg' case, medullary blood flow reflects the decrease in renal blood flow at lower temperature (Fig. 8c). The competing effects of reduced oxygen consumption and reduced oxygen supply result in a relatively constant medullary P_{O2} and decreasing urinary P_{O2} at sufficiently lower temperatures. Predictions of the 'partial autoreg' case lie between the two extreme cases.

3.3 *Renal oxygenation under CPB*

In the next set of simulations, we aim to identify the phase of the cardiac surgery performed under CPB when the kidney is most vulnerable to hypoxic injury. As in our previous study (Sgouralis *et al.*, 2015), four CPB phases were considered: (i) pre-CPB, defined as the period following induction of anaesthesia

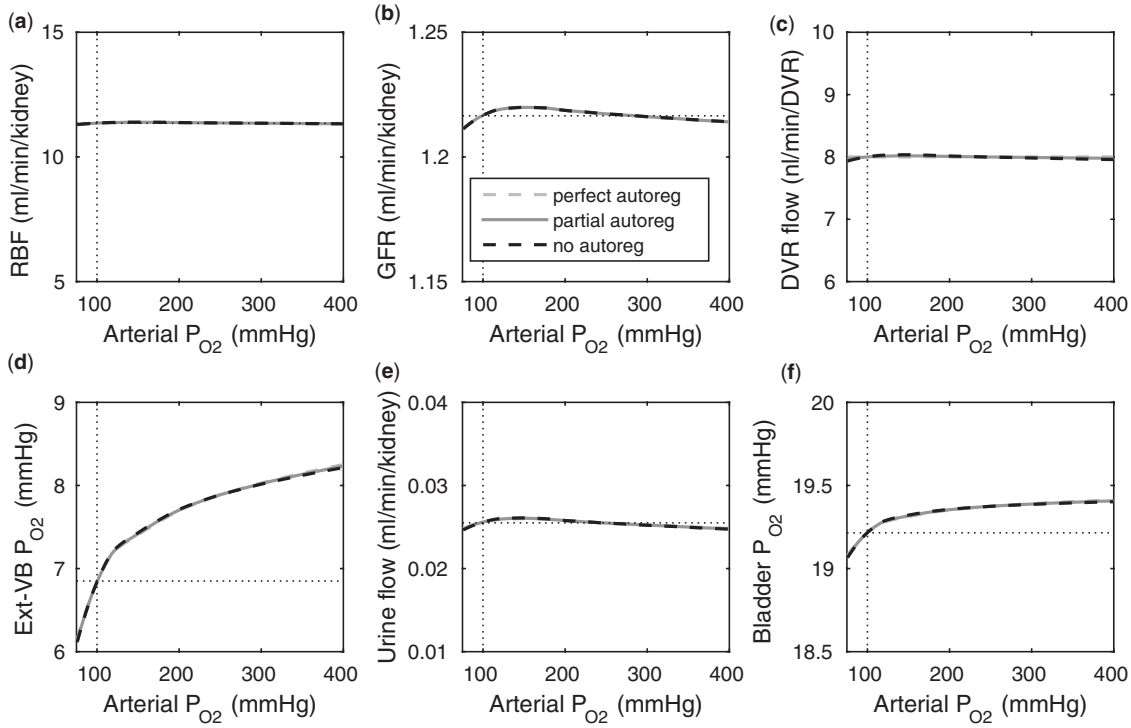

FIG. 7. Effects of variations in arterial P_{O2} on: (a) renal blood flow; (b) glomerular filtration rate; (c) DVR flow at the cortico-medullary boundary; (d) interstitial fluid P_{O2} in the lower inner stripe outside the vascular bundles; (e) urine flow and (f) urinary P_{O2} in the bladder. Results were computed for three different scenarios of medullary blood flow autoregulation. Dotted lines indicate baseline values.

and prior to initiation of CPB; (ii) CPB-hypothermia, the hypothermic period of the surgery (iii) CPB-rewarming, the normothermic period of the surgery; and (iv) post-CPB, the post-surgical period in which the effects of haemodilution and anaesthesia persist. Because of the uncertainty on the degree of medullary blood flow autoregulation, we repeated every simulation for the three cases of Section 3.2. Namely, these cases are 'perfect autoreg', 'partial autoreg', and 'no autoreg'.

Model parameters for the CPB phases are given in Table 1. The chosen values are typical of those encountered during CPB in humans (Andersson *et al.*, 1994). In particular, during the hypothermic CPB phase, body temperature is lowered to 28°C.[1] Other differences among the four CPB phases include:

(1) In part due to the effects of anaesthesia, RPP is lower than baseline in all four phases but particularly so during the hypothermic and rewarming phases during which the patient's circulation is externally driven (Andersson *et al.*, 1994).

(2) Except for the pre-CPB phase, systemic haematocrit is substantially lower than normal due to the requirement of a priming solution within the extracorporeal circuit (Andersson *et al.*, 1994).

[1]Patient body temperature is lowered to different degrees depending on the nature of the surgery and varies between institutions. The model predicts qualitatively similar results (not shown) at different body temperatures.

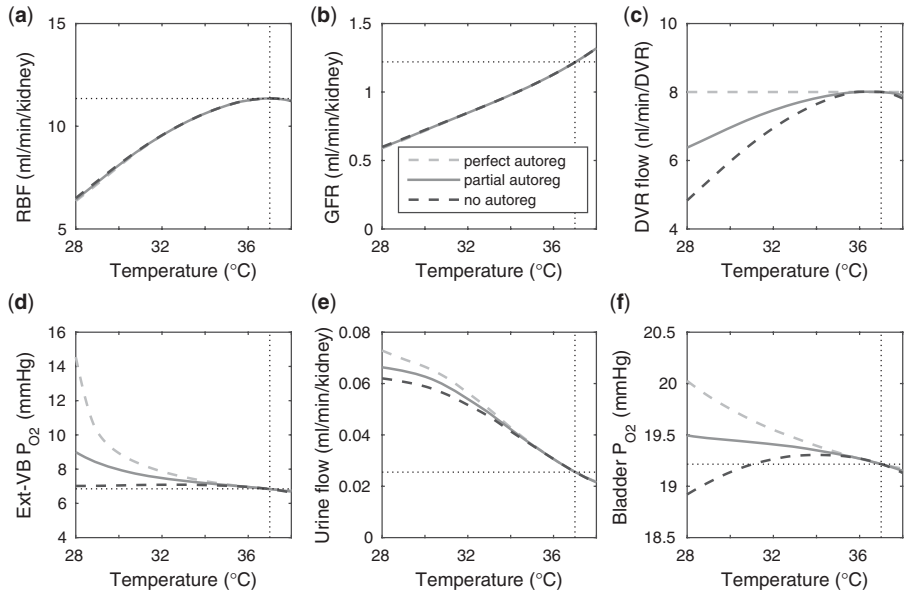

FIG. 8. Effects of variations in body temperature on (a) renal blood flow; (b) glomerular filtration rate; (c) DVR flow at the cortico-medullary boundary; (d) interstitial fluid P_{O2} in the lower inner stripe outside the vascular bundles; (e), urine flow and (f), urinary P_{O2} in the bladder. Results were computed for three different scenarios of medullary blood flow autoregulation. Dotted lines indicate baseline values.

(3) During the hypothermic and rewarming CPB phases, the impact of haemodilution on oxygen delivery is partially compensated by the ventilation of the patient with almost 100% oxygen.

A comparison of renal oxygenation is shown on Fig. 9. One may view the P_{O2} of the extra-bundle region in the inner stripe as an indicator for the risk of AKI, inasmuch as the inner stripe is the least oxygenated region of the outer medulla and contains the vulnerable medullary TALs. In terms of the relative risk for AKI during the CPB phases, it is interesting that the model yields rather different predictions depending on the degree to which medullary blood flow is regulated.

Pre-CPB phase. When perfect medullary blood flow autoregulation is assumed, the model predicts slight reductions during the pre-CPB phase in the inner stripe, CD and bladder urine P_{O2} ($\sim$0.2, 0.2, 0.1 mmHg, respectively). The pre-CPB phase differs from baseline only in having a lower RPP (75 vs. 100 mmHg), which, owing to the compensatory response of the autoregulatory mechanisms, results in minimal change in glomerular filtration rate and no change in medullary blood flow (fixed in the 'perfect autoreg' case). Reductions in P_{O2} become more substantial as the degree of autoregulation decreases. In the absence of medullary blood flow autoregulation, the pre-CPB phase is predicted to yield substantially lower medullary and bladder urine P_{O2} than baseline ($\sim$0.6 and 0.2 mmHg, respectively). At a RPP of 75 mmHg, the 'no autoreg' model predicts 9% and 8% reductions in medullary blood flow and glomerular filtration rate, respectively. Together, these changes result in a 12% reduction in inner-stripe interstitial fluid P_{O2}.

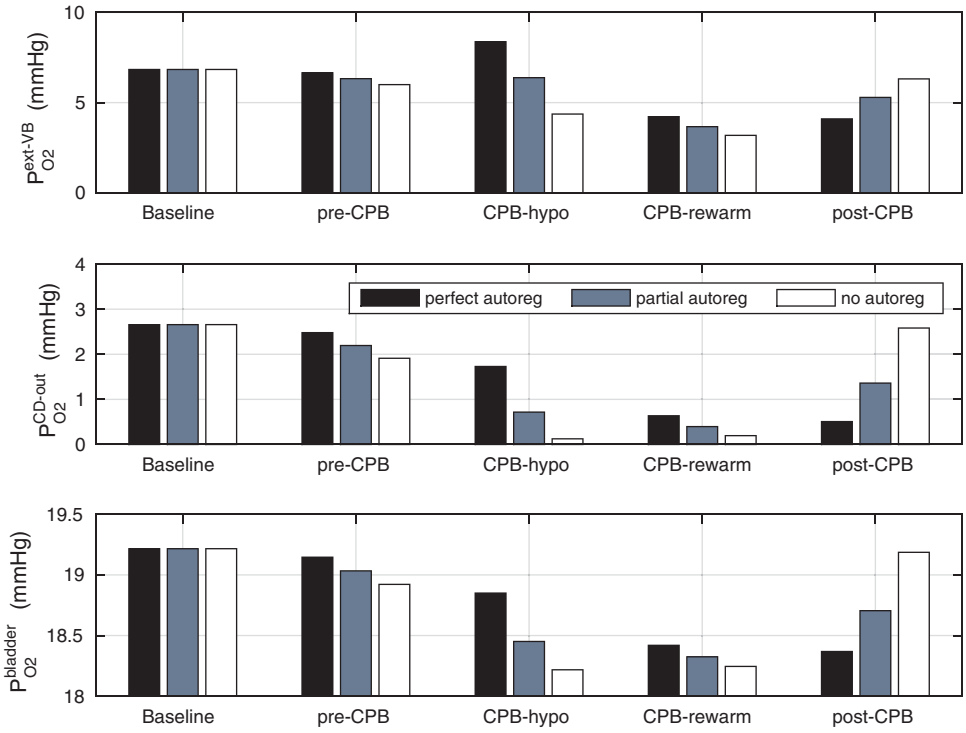

FIG. 9. Renal oxygenation during CPB surgery. Top panel, interstitial fluid P_{O2} in the interbundle region in the lower inner stripe of the outer medulla. Middle panel, fluid P_{O2} at the CD outlet (i.e. renal pelvis). Bottom panel, urinary P_{O2} in the bladder. Results were obtained for the five phases of Table 1 each for three different degrees of medullary blood flow regulation.

CPB-hypothermic phase. Haemodilution begins during the hypothermic phase of CPB. Taken in isolation, the lower blood viscosity in haemodilution would increase blood flow. However, during surgery RPP is further reduced to 50 mmHg, at which point renal autoregulation can no longer compensate for the pressure variations and stabilize glomerular filtration rate. Altogether, these factors result in a 39% reduction in arteriolar blood flow and a 62% reduction in glomerular filtration rate. With medullary blood flow fixed ('perfect autoreg'), haemodilution leads to a 45% reduction in medullary oxygen delivery. But interestingly, the model predicts that inner-stripe P_{O2} is the highest during the hypothermic CPB phase. In fact, the predicted inner-stripe P_{O2} exceeds even that of base case. This counter-intuitive result may be attributed to hypothermia, which substantially reduces active Na^+ transport and oxygen consumption and to the model's assumption that medullary blood flow remains at baseline value. In the hypothermic CPB phase, the oxygen consumption due to thick limb active Na^+ drops drastically to 13% that of base case. Thus, even with haemodilution, the model predicts that only 23% of the medullary oxygen supply is consumed, with the net result being an increase in medullary oxygen levels. However, P_{O2} of the CD outflow and bladder urine are lower than base case. This is because the hypothermia induced reduction in TAL Na^+ transport impairs water reabsorption from water-permeable nephron segments and leads to diuresis, which limits the concentration (but not the amount) of oxygen in the CD.

The prediction in the 'perfect autoreg' case that during the hypothermic CPB phase medullary P_{O2} exceeds even baseline seems rather counter-intuitive and is indeed inconsistent with model predictions

when medullary blood flow is insufficiently autoregulated. As previously noted, at RPP of 50 mmHg, renal autoregulation fails to compensate. Even with a reduced blood viscosity due to haemodilution, medullary blood flow decreases to 6.5 and 4.8 nl/min/DVR in the 'partial autoreg' and 'no autoreg' cases, respectively, compared to 8 nl/min/DVR in the base case (or 'perfect autoreg' case). For the 'no autoreg' case, the lowered medullary blood flow and hemodilution decrease medullary oxygen delivery to 34% of baseline. This is accompanied by a 27% reduction in oxygen consumption by the TALs, induced by the lowering of body temperature to 28°C. Together, these factors result in medullary oxygen extraction of 55% and an inner-stripe interstitial fluid P_{O2} of 4.3 mmHg, which is 36% lower than baseline. Bladder urine P_{O2} decreases from its baseline value of 19.1 to 18.3 mmHg. The analogous inner-stripe and bladder urine P_{O2} are predicted to be 6.3 and 18.5 mmHg, respectively, for the 'partial autoreg' case.

CPB-rewarming and post-CPB phases. With the transition to the rewarming phase of CPB, body temperature is restored to 37°C. A particularly notable effect of a higher body temperature is the increase in TAL active transport of Na^+. Consequently, medullary oxygen consumption is ∼50% greater than in the hypothermic phase of CPB. The 'perfect autoreg' case predicts that the lowest inner-stripe P_{O2} is obtained during the CPB rewarming and post-CPB phases (4.2 and 4.1 mmHg, respectively). Here, oxygen demand increases as body temperature is raised, but medullary oxygen levels remain low due to haemodilution; consequently, medullary oxygen extraction increases to 83%. The same trend can be seen in the P_{O2} of collecting duct outflow, which drops to ∼0.7 and ∼0.5 mmHg, and bladder urine, which drops to ∼18.4 and ∼18.3 mmHg, respectively. Thus, the model predicts that if the autoregulation of medullary blood flow is perfect during the surgery, then the patient is at similarly high risk of AKI during the rewarming and the post-CPB phases.

When medullary blood flow autoregulation is less than perfect, the model predicts substantially different P_{O2} levels in the CPB rewarming and post-CPB phases. Both the 'partial autoreg' case and the 'no autoreg' case predict that the rewarming phase, during which RPP remains low at 50 mmHg, yields the lowest inner-stripe P_{O2} (3.7 and 3.1 mmHg, respectively, compared to 6.8 mmHg in baseline) among all four phases and a low bladder urine P_{O2} (18.4 and 18.3 mmHg, respectively, compared to 19.1 mmHg in baseline). It is noteworthy that in the 'no autoreg' case the CD outflow and bladder urine P_{O2} values are slightly higher in the rewarming phase than in the hypothermic phase, even though the inner-stripe P_{O2} is lower in the rewarming phase. This discrepancy can be attributed to the higher TAL Na^+ transport in the rewarming phase, which results in a lower Na^+ load downstream and consequently lower Na^+ active transport and oxygen consumption along the inner-medullary CD.

In the post-CPB phase, medullary blood flow increases in the 'partial autoreg' and 'no autoreg' cases as RPP is restored to the pre-CPB levels. Consequently, the model predicts inner-stripe, CD outflow and bladder urinary P_{O2} that are slightly lower than baseline and that are more similar to the pre-CPB levels.

In summary, the model simulations suggest that the extent to which medullary blood flow is autoregulated may have a substantial impact on the relative risk of medullary hypoxic injury during the different phases of the cardiac surgery.

The relationship between inner-stripe extrabundle interstitial P_{O2} and bladder urine P_{O2} during the different CPB phases is summarized in Fig. 10. Generally, low medullary P_{O2} values are associated with low bladder urinary P_{O2} values. However, the precise relationship depends on the prevailing systemic factors of each phase. Further, the degree of medullary blood flow autoregulation induces a substantial variation in the predicted relationship, especially during the hypothermic and post-surgical phases.

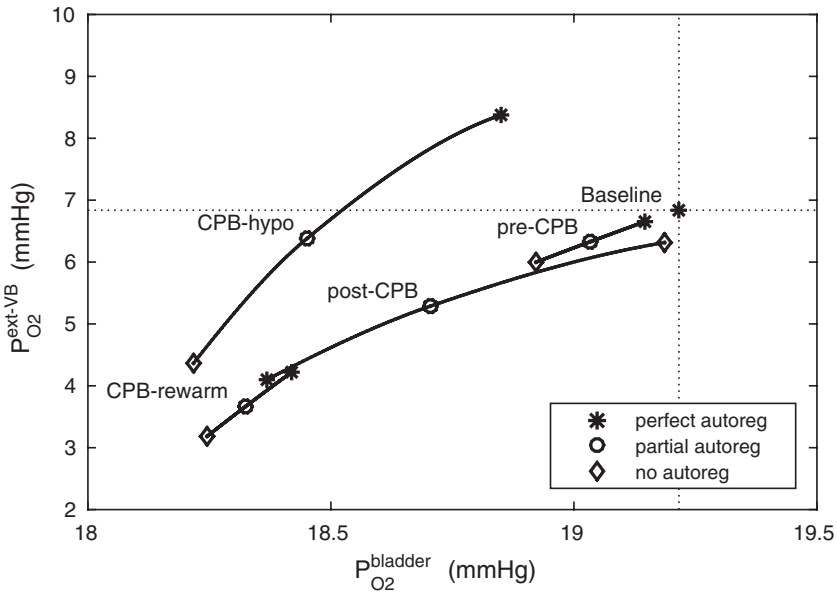

FIG. 10. Relationship between lower inner stripe P_{O2} and urinary bladder P_{O2}. Results were obtained for the five phases of Table 1 each for different degrees of medullary blood flow regulation that ranges from $\beta = 0$ (perfect autoreg) to $\beta = 100\%$ (no autoreg).

4. Discussion

Despite receiving approximately 25% of the cardiac output, the mammalian kidney is susceptible to hypoxia. The low medullary P_{O2} may be attributable, in part, to the high metabolic demand of the Na^+/K^+-ATPase pumps, which accounts for the majority of the energy consumption in the kidney. A principal goal of this study was to determine regional P_{O2} in a rat kidney and urinary tract. Of particular interest are the inner stripe, the papillary tip and the bladder. In the inner stripe of the rodent kidney, the oxygen-carrying DVR are isolated within tightly packed vascular bundles, separated from the metabolically demanding TALs. The structural organization of the tubules and vessels, which has been identified in rats, mice and human (Kriz, 1967; Kriz *et al.*, 1972; Kriz & Koepsell, 1974; Jamison & Kriz, 1982), likely results in a substantial radial gradient in P_{O2}. The present model indeed predicts such a radial gradient in interstitial P_{O2}, from an average of ∼30 mmHg in the core of the vascular bundle, to an average P_{O2} of ∼7.5 mmHg in the interbundle region, Fig. 4a.

Under baseline conditions, the DVR deliver ∼23% of the medullary oxygen supply to the inner medulla. Thus, P_{O2} in the inner medulla is even lower than in the outer medulla. The model predicts that, under baseline conditions, urinary P_{O2} at the papillary tip is 2.4 mmHg, which is 4.1 mmHg below the interstitial fluid P_{O2} near the inner-outer medullary boundary. Along the ureter, urine becomes increasingly oxygenated owing to oxygen diffusion, reaching a P_{O2} of 19.1 mmHg in the Fig. 4b. These results point to a large difference in bladder urinary P_{O2} and medullary P_{O2}.

The predicted medullary P_{O2} is in general agreement with tissue P_{O2} measured in the rat kidney, at least under the relatively antidiuretic conditions modelled in this study (Epsteinein *et al.*, 1994; Palm *et al.*, 2003). In contrast, substantially higher medullary tissue P_{O2} (∼30 mmHg) has been reported in unanaesthetized sheep (Calzavacca *et al.*, 2015). Similarly high renal pelvic urine P_{O2} values have been

reported in anaesthetized dogs (27 mmHg) (Rennie *et al.*, 1958) and in humans (28 mmHg) (Lenhardt & Landes, 1963). Notably, Lenhardt & Landes (1963) reported that urinary P_{O2} *decreases* along the ureter, in direct contradiction with our model's prediction, which indicates a substantial *increase* (see Fig. 4b). Indeed, on the basis of their findings, Lenhardt & Landes (1965) concluded that urinary P_{O2} 'reflects the interstitial P_{O2} in the medulla,' again in contrast to our conclusion. These discrepancies suggest that there may be fundamental differences in renal haemodynamics and medullary oxygenation between the rat and larger animals like sheep and human. For example, given the low tissue P_{O2} in the inner medulla (∼10 mmHg) (Epsteinein *et al.*, 1994), it seems unlikely that pelvic urinary P_{O2} can rise to 50 mmHg, the value measured in human (Lenhardt & Landes, 1963). To reconcile these differences, one would need a better understanding of the anatomic structures and of renal and medullary blood flow autoregulation in humans. It should also be noted that there are very little available data regarding the relative changes in medullary and urinary P_{O2} that occur under physiological and pathophysiological conditions. However, a recent study in unanaesthetized sheep showed a strong correlation between tissue P_{O2} in the medulla and the P_{O2} of urine in the bladder during development of septic AKI (Lankadeva *et al.*, 2016). Thus, the potential for urinary P_{O2} to be used as a biomarker of risk of AKI may still merit further investigation.

Another goal of this study was to determine the phase or phases of cardiac surgery performed under CPB during which the outer medulla and the TALs are most susceptible to hypoxia and the underlying renal haemodynamic and functional factors that contribute to this susceptibility. Given the low baseline medullary P_{O2}, the TALs likely operate near anoxia. Thus, a clinically important question is: When renal oxygen delivery is reduced during cardiac surgery performed under CPB, how likely are the thick limbs to become hypoxic?

Model simulations suggest that the outer medulla's relative vulnerability to hypoxic injury during the different phases of the surgery depends, in part, on the extent to which medullary blood flow is autoregulated. There is evidence that indicates a link between increased renal interstitial hydrostatic pressure and elevated medullary blood flow, which is in turn modulated by vasopressin, the antidiuretic hormone (Cowley, 2000). In general, medullary blood flow is known to be strongly autoregulated in antidiuretic rats (Cupples & Marsh, 1988; Mattson *et al.*, 1993; Franchini *et al.*, 1997) and weakly regulated in diuretic rats (Roman *et al.*, 1988; Mattson *et al.*, 1991; Franchini *et al.*, 1997). However, the degree to which medullary blood flow is regulated when a patient or an animal is undergoing surgery performed under CPB is not well characterized.

If medullary blood flow is perfectly autoregulated, then outer medullary P_{O2} is predicted to be the lowest during the rewarming and post-surgical phases of CPB, when medullary oxygen supply is low due to haemodilution but medullary oxygen consumption remains high (Fig. 9). The model predicts that during the rewarming phase 83% of the medullary oxygen supply is consumed, resulting in tubular fluid P_{O2} as low as 2.3 mmHg in the inner-stripe segment of the superficial TALs. Similar results were obtained for the post-CPB phase. It is noteworthy that even though medullary oxygen supply exceeds consumption by a comfortable margin, the risk of medullary hypoxia can still be substantial. This apparent paradox is explained by the anatomic structure of the outer medulla, as discussed above. However, with medullary blood flow assumed fixed, the model yields the somewhat counter-intuitive prediction that during the hypothermic CPB phase, when medullary TAL transport and oxygen consumption dramatically decrease, medullary oxygenation exceeds baseline levels (Fig. 9).

In contrast, if the assumption of perfect autoregulation is relaxed so that medullary blood flow is linked to renal blood flow, then model simulations identify the rewarming phase of CPB, in which medullary blood flow is low but medullary oxygen consumption remains high, as the phase in which the kidney is the most vulnerable to hypoxic injury (Fig. 9). The model predicts that during the rewarming phase of

CPB, 93% of the medullary O_2 supply is consumed, resulting, in the 'no autoreg' case, P_{O2} of 1.6 and 3.2 mmHg in the TAL luminal fluid and the surrounding interstitial fluid, respectively.

Renal tubules consist of a single layer of epithelial cells, with different transporters expressed on the apical and basolateral membranes. For example, for Na^+ to be reabsorbed by the TALs, it may go through either the transcellular or paracellular pathway. For transcellular transport, the Na^+ must first pass through the apical membrane (likely via the Na^+-K^+-2 Cl^- or NKCC, transporter) and then through the basolateral membrane (likely via the Na^+-K^+-ATPase). Alternatively, the Na^+ may be reabsorbed through the tight junction, driven by a favourable electrochemical gradient. In contrast, for simplicity the present model represents single-barrier transport, where TAL Na^+ transport is determined by the Michaelis–Menten kinetics. Thus, the model cannot distinguish between transcellular transport (which consumes O_2) and paracellular transport (which does not). Instead, it assumes that the TQ ratio is known *a priori*. This limitation applies to all nephron segments that engage in active Na^+ transport. To overcome this limitation and to improve the accuracy of the predicted T_{Na} and Q_{O2}, the model nephron could be replaced by an epithelial-based model (e.g. Edwards *et al.*, 2014; Layton *et al.*, 2016), although this extension is by no means trivial.

As previously noted, there appears to be substantial differences between the predictions of the present model, which is based on a rat kidney, and measurements in human. In fact, urine P_{O2} in patients undergoing cardiac surgery performed on CPB was measured to be >50 mmHg (Kainuma *et al.*, 1996). It is clear that there are important differences between the rat and human kidneys beyond their sizes. Because of the scarcity of data (anatomic, transport, electrochemical, etc.) in the human kidney relative to the rat, all detailed mathematical models of the mammalian kidney have been built for the rat (Chen *et al.*, 2009; Layton, 2011; Layton & Layton, 2011; Edwards & Layton, 2012, 2014; Layton & Bankir, 2013; Weinstein, 2015a,b). Nonetheless, the large discrepancies between the rat model and human data clearly indicate the limit of knowledge that one can gain from a rat model and that a better understanding of the relationship between urinary and medullary P_{O2} in the human kidney might benefit from a model of the human kidney.

Funding

This work was conducted while I.S. is a Postdoctoral Fellow at the National Institute for Mathematical and Biological Synthesis, an Institute sponsored by the National Science Foundation through NSF Award DBI1300426, with additional support from the National Institutes of Health, National Institute of Diabetes and Digestive and Kidney Diseases, via grant R01DK089066 to A.L.

Supplementary material

Supplementary material is available at http://imammb.oxfordjournals.org.

References

Andersson, L. G., Bratteby, L. E., Ekroth, R., Hallhagen, S., Joachimsson, P. O., van der Linden, J. & Wesslén, O. (1994) Renal function during cardiopulmonary bypass: influence of pump flow and systemic blood pressure. *Eur. J. Cardiothorac. Surg.*, **8**, 597–602.

Bjornsson, T. D. (1979) Use of serum creatinine concentrations to determine renal function. *Clin. Pharmacokinet.*, **4**, 200–22, 1979.

Bosch, J. P. (1995) Renal reserve: a functional view of glomerular filtration rate. *Semin. Nephrol.*, **15**, 381–5.

Brezis, M. & Rosen, S. (1995) Hypoxia of the renal medulla—its implications for disease. *N. Engl. J. Med.*, **332**, 647–655.

Broman, M. & Källskog, O. (1995) The effects of hypothermia on renal function and haemodynamics in the rat. *Acta Physiol. Scand.*, **153**, 179–84.

Calzavacca, P., Evans, R. G., Bailey, M., Lankadeva, Y. R., Bellomo, R. & May, C. N. (2015) Long-term measurement of renal cortical and medullary tissue oxygenation and perfusion in unanesthetized sheep. *Am. J. Physiol. Regu. Integr. Comp. Physiol.*, **308**, R832–R839.

Chen, J., Layton, A. T. & Edwards, A. (2009) A mathematical model of oxygen transport in the rat outer medulla: I. model formulation and baseline results. *Am. J. Physiol. Renal. Physiol.*, **297**, F517–F536.

Chen, J., Sgouralis, I., Moore, L. C., Layton, H. E. & Layton, A. T. (2011) A mathematical model of the myogenic response to systolic pressure in the afferent arteriole. *Am. J. Physiol. Renal. Physiol.*, **300**, F669–81.

Cowley, A. W., Jr. (2000) Control of the renal medullary circulation by vasopressin v1 and v2 receptors in the rat. *Exp. Physiol.*, **85**, 223–231.

Cupples, W. A. & Marsh, D. J. (1988) Autoregulation of blood flow in renal medulla of the rat: no role for angiotensin II. *Can. J. Physiol. Pharmacol.*, **66**, 833–836.

Edwards, A. & Layton, A. T. (2012) Impacts of nitric oxide-mediated vasodilation on outer medullary NaCl transport and oxygenation. *Am. J. Physiol. Renal. Physiol.*, **303**, F907–17.

Edwards, A. & Layton, A. T. (2014) Calcium dynamics underlying the afferent arteriole myogenic response. *Am. J. Physiol. Renal. Physiol.*, **306**, F34–F48.

Edwards, A., Castrop, H., Laghmani, K., Vallon, V. & Layton, A. T. (2014) Effects of NKCC2 isoform regulation on nacl transport in thick ascending limb and macula densa: a modeling study. *Am. J. Physiol. Renal. Physiol.*, **307**, F137–F146.

Epsteinein, F. H., Agmon, Y. & Brezis, M. (1994) Physiology of renal hypoxia. *Ann. N. Y. Acad. Sci.*, **718**, 72—82.

Evans, R. G., Ince, C., Joles, J. A., Smith, D. W., May, C. N., O'Connor, P. M. & Gardiner, B. S. (2013) Haemodynamic influences on kidney oxygenation: clinical implications of integrative physiology. *Clin. Exp. Pharmacol. Physiol.*, **40**, 106–22.

Evans, R. G., Smith, J. A., Wright, C., Gardiner, B. S., Smith, D. W. & Cochrane, A. D. (2014) Urinary oxygen tension: a clinical window on the health of the renal medulla? *Am. J. Physiol. Regul. Integr. Comp. Physiol.*, **306**, R45–50.

Franchini, K. G., Mattson, D. L. & Cowley, A. W., Jr. (1997) Vasopressin modulation of medullary blood flow and pressure-natriuresis-diuresis in the decerebrated rat. *Am. J. Physiol. Regul. Integr. Comp. Physiol.*, **272**, R1472–R1479.

Fry, B. C., Edward, A., & Layton, A. T. (2015) Impact of nitric oxide and superoxide on renal medullary oxygen transport and urine concentration. *Am. J. Physiol. Renal. Physiol.*, **308**, F967–F980.

Fry, B. C., Edwards, A., Sgouralis, I. & Layton, A. T. (2014) Impact of renal medullary three-dimensional architecture on oxygen transport. *Am. J. Physiol. Renal. Physiol.*, **307**, F263–72.

Herrera, J. & Rodríguez-Iturbe, B. (1998) Stimulation of tubular secretion of creatinine in health and in conditions associated with reduced nephron mass. Evidence for a tubular functional reserve. *Nephrol. Dial. Transplant.*, **13**, 623–9.

Jamison, R. L. & Kriz, W. (1982) *Urinary Concentrating Mechanism: Structure and Function*. New York: Oxford University Press.

Kainuma, M., Yamada, M. & Miyake, T. (1996) Continuous urine oxygen tension monitoring in patients undergoing cardiac surgery. *J. Cardiothorac. Vasc. Anesth.*, **10**, 603–608.

Karkouti, K., Wijeysundera, D. N., Yau, T. M., Callum, J. L., Cheng, D. C., Crowther, M., Dupuis, J.-Y., Fremes, S. E., Kent, B., Laflamme, C., Lamy, A., Legare, J.-F., Mazer, C. D., McCluskey, S. A., Rubens, F. D., Sawchuk, C. & Beattie, W. S. (2009) Acute kidney injury after cardiac surgery: focus on modifiable risk factors. *Circulation*, **119**, 495–502.

Kreft, M. E., Hudoklin, S., Jezernik, K. & Romih, R. (2010) Formation and maintenance of blood-urine barrier in urothelium. *Protoplasma*, **246**, 3–14.

Kriz, W. (1967) Der architektonische and funktionelle Aufbau der Rattenniere. *Z. Zellforsch.*, **82**, 495–535.

Kriz, W. & Koepsell, H. (1974) The structural organization of the mouse kidney. *Z. Anat. Entwickl.-Gesch.*, **144**, 137–163.

KRIZ, W., SCHNERMANN, J. & KOEPSELL, H. (1972) The position of short and long loops of Henle in the rat kidney. *Z. Anat. Entwickl.-Gesch.*, **138**, 301–319.

LANKADEVA, Y., KOSAKA, J., EVANS, R., BAILEY, S., BELLOMO, R. & MAY, C. (2016) Intra-renal and urinary oxygenation during norepinephrine resuscitation in ovine septic acute kidney injury. *Kidney Int*.

LAYTON, A. T., VALLON, V. & EDWARDS, A. (2016) Predicted consequences of diabetes and SGLT inhibition on transport and oxygen consumption along a rat nephron. *Am. J. Physiol. Renal. Physiol.*, ajprenal–00543, 2016.

LAYTON, A. T. (2011) A mathematical model of the urine concentrating mechanism in the rat renal medulla: I. Formulation and base-case results. *Am. J. Physiol. Renal. Physiol.*, **300**, F356–F371.

LAYTON, A. T. & BANKIR, L. (2013) Impacts of active urea secretion into pars recta on urine concentration and urea excretion rate. *Physiol. Rep.*, **1**, e00034.

LAYTON, A. T., DANTZLER, W. H. & PANNABECKER, T. L. (2012) Urine concentrating mechanism: impact of vascular and tubular architecture and a proposed descending limb urea-na+ cotransporter. *Am. J. Physiol. Renal. Physiol.*, **302**, F591–605.

LAYTON, A. T. & LAYTON, H. E. (2011) Countercurrent multiplication may not explain the axial osmolality gradient in the outer medulla of the rat kidney. *Am. J. Physiol. Renal. Physiol.*, **301**, F1047–F1056.

LENHARDT, K. O. & LANDES, R. R. (1963) Oxygen tension of the urine and renal structures. *N. Eng. J. Med.*, **269**, 115–121.

LENHARDT, K. O. & LANDES, R. R. (1965) Urinary oxygen pressure in renal parenchymal and vascular disease. *J. Am. Med. Assoc.*, **194**, 345–350.

MATTSON, D. L., LU, S., ROMAN, R. J. & COWLEY, A. W., JR. (1993) Relationship between renal perfusion pressure and blood flow in different regions of the kidney. *Am. J. Physiol. Regul. Integr. Comp. Physiol.*, **264**, R578–R583.

MATTSON, D. L., RAFF, H. & ROMAN, R. J. (1991) Influence of angiotensin II on pressure natriuresis and renal hemodynamics in volume-expanded rats. *Am. J. Physiol. Regul. Integr. Comp. Physiol.*, **260**, R1200–R1209.

MEHTA, R. L. & CHERTOW, G. M. (2003) Acute renal failure definitions and classification: time for change? *J. Am. Soc. Nephrol.*, **14**, 2178–87.

MOSS, R. & LAYTON, A. T. (2014) Dominant factors that govern pressure natriuresis in diuresis and antidiuresis: a mathematical model. *Am. J. Physiol. Renal. Physiol.*, **306**, F952–69.

NIEVES-GONZALEZ, A., CLAUSEN, C., LAYTON, A. T., LAYTON, H. E. & MOORE, L. C. (2013) Transport efficiency and workload distribution in a mathematical model of the thick ascending limb. *Am. J. Physiol. Renal. Physiol.*, **304**, F653–F664.

OKUSA MD, M. D., LINDEN, J., MACDONALD, T. & HUANG, L. (1999) Selective A2A adenosine receptor activation reduces ischemia-reperfusion injury in rat kidney. *Am. J. Physiol. Renal. Physiol.*, **277**, F404–F412.

ONYEANUSI, B. I., ADENIYI, A. A., AYO, J. O., IBE, C. S., ONYEANUSI, C. G., ET AL. (2009) A comparative study of the urinary system of the African giant rat (Cricetomys gambianus Waterhouse) and the Wistar rat. *Pak. J. Nutr.*, **8**, 1043–1047.

PALM, F., CEDERBERG, J., HANSELL, P., LISS, P. & CARLSSON, P. O. (2003) Reactive oxygen species cause diabetes-induced decrease in renal oxygen tension. *Diabetologia*, **46**, 1153–1160.

PANNABECKER, T. L., ABBOTT, D. E. & DANTZLER, W. H. (2004) Three-dimensional functional reconstruction of inner medullary thin limbs of Henle's loop. *Am. J. Physiol. Renal. Physiol.*, **286**, F38–F45.

PRIES, A. R., SECOMB, T. W., GESSNER, T., SPERANDIO, M. B., GROSS, J. F. & GAEHTGENS, P. (1994) Resistance to blood flow in microvessels in vivo. *Circ. Res.*, **75**, 904–15.

RENNIE, D. W., REEVES, R. B. & PAPPENHEIMER, J. R. (1958) Oxygen pressure in urine and its relation to intrarenal blood flow. *Am. J. Physiol*, **195**, 120–132.

ROMAN, R J., COWLEY JR, A. W., GARCIA-ESTAN, J. & LOMBARD, J. H. (1988) Pressure-diuresis in volume-expanded rats, cortical and medullary hemodynamics. *Hypertension*, **12**, 168–176.

ROSNER, M. H., PORTILLA, D. & OKUSA, M. D. (2008) Cardiac surgery as a cause of acute kidney injury: pathogenesis and potential therapies. *J. Intensive Care Med.*, **23**, 3–18.

SGOURALIS, I., EVANS, R. G., GARDINER, B. S., SMITH, J. A., FRY, B. C. & LAYTON, A. T. (2015) Renal hemodynamics, function & oxygenation during cardiac surgery performed on cardiopulmonary bypass: a modeling study. *Physiol. Rep.*, **3**, e12260.

SGOURALIS, I. & LAYTON, A. T. (2013) Control and modulation of fluid flow in the rat kidney. *Bull. Math. Biol.*, **75**, 2551–74.

SGOURALIS, I. & LAYTON, A. T. (2014) Theoretical assessment of renal autoregulatory mechanisms. *Am. J. Physiol. Renal. Physiol*, **306**, F1357–71.

SGOURALIS, I. & LAYTON, A. T. (2015a) Conduction of feedback-mediated signal in a computational model of coupled nephrons. *Math. Med. Biol*, **33**, 87–106.

SGOURALIS, I. & LAYTON, A. T. (2015b) Mathematical modeling of renal hemodynamics in physiology and pathophysiology. *Math. Biosci.*, **264**, 8–20.

SGOURALIS, I., KOSAKA, J., EVANS, R., BAILEY, S., BELLOMO, R. & MAY, C. (2012) Autoregulation and conduction of vasomotor responses in a mathematical model of the rat afferent arteriole. *Am. J. Physiol. Renal. Physiol.*, **303**, F229–39.

STAR, R. A. (1998) Treatment of acute renal failure. *Kidney Int.*, **54**, 1817–31.

TILLIG, B. & CONSTANTINOU, C. E. (1996) Videomicroscopic imaging of ureteral peristaltic function in rats during cystometry. *J. Pharmacol. Toxicol. Methods*, **35**, 191–202.

WEINSTEIN, A. M. (1998) A mathematical model of the inner medullary collecting duct of the rat: pathways for Na and K transport. *Am. J. Physiol. (Renal. Physiol.* 43*)*, **274**, F841–F855.

WEINSTEIN, A. M. (2015a) A mathematical model of rat proximal tubule and loop of Henle. *Am. J. Physiol. Renal. Physiol.*, **308**, F1076–F1097.

WEINSTEIN, A. M. (2015b) A mathematical model of the rat nephron: glucose transport. *Am. J. Physiol. Renal. Physiol.*, **308**, F1098–F1118.

WOLF, J. S., HUMPHREY, P. A., RAYALA, H. J., GARDNER, S. M., MACKEY, R. B. & CLAYMAN, R. V. (1996) Comparative ureteral microanatomy. *J. Endourol.*, **10**, 527–531.